

Analysis of a Large Number of Vias and Differential Signaling in Multilayered Structures

Houfei Chen, Qin Li, Leung Tsang, *Fellow, IEEE*, Chung-Chi Huang, and Vikram Jandhyala, *Member, IEEE*

Abstract—A method is presented for full-wave modeling of vertical vias in multilayered integrated circuits. The analysis of the interior problem is based upon the cylindrical wave expansion of the magnetic field Green's function. The multiple interaction among vertical vias is modeled by the Foldy–Lax scattering formula. Multilayered effects are included by using cascaded network of the single-layer components. The exterior problem of the via and the transmission line is analyzed using the method of moments approach. The exterior and interior problems are combined into a system of equations to facilitate the solution of a large number of vias. Using this approach, the scattering matrix of problems of several thousand vias can be calculated with moderate CPU and memory requirement. Numerical results have been obtained for different via configurations and for a large range of frequency. Also illustrated are results for common and differential mode in differential signaling with surrounding idle and shorting vias.

Index Terms—Differential signaling, scattering parameter, via-coupling.

I. INTRODUCTION

BECAUSE OF THE ever-increasing speed, density, and routing complexity in integrated circuit (IC) design, via structure is extensively used to connect signal traces residing on different layers. The impedance difference between vias and signal traces introduces reflection. The nature of the multilayered geometry introduces the parallel plate waveguide effect, which results in significant coupling among vias. Coupling through parallel plate waveguide modes generally decays slowly as the square root of distance and poses a significant challenge to reliable, high-speed IC operation. Numerous problems arising there (such as larger delays, loss of signal integrity, and false switching of devices) can lead to the malfunctioning of overall systems.

In the past, different types of vias have been investigated using various methods. The inductance of a via connection of two striplines was analyzed [1] by using the partial electric element circuit (PEEC) model [2]. The capacitance and inductance of a through-hole via has been analyzed using the quasi-static

Manuscript received January 7, 2002; revised October 4, 2002. This work was supported by the Washington Technology Center, HyperLynx, the Intel Corporation, and the City University of Hong Kong through Research Project 9380034.

H. Chen was with the Department of Electrical Engineering, University of Washington, Seattle, WA 98195 USA. He is now with the Advance System Research Laboratory, MICRON, Boise, ID 83707 USA.

Q. Li, C.-C. Huang, and V. Jandhyala are with the Department of Electrical Engineering, University of Washington, Seattle, WA 98195 USA.

L. Tsang is with the Department of Electrical Engineering, University of Washington, Seattle, WA 98195 USA and also with the Department of Electronic Engineering, City University of Hong Kong, Hong Kong.

Digital Object Identifier 10.1109/TMTT.2003.808616

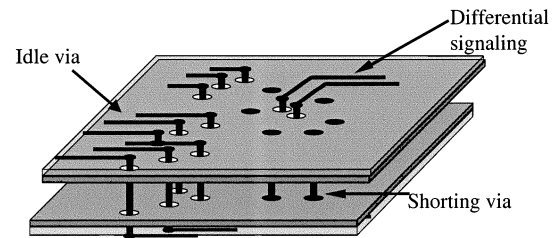


Fig. 1. Typical multi-via structure including a pair of differential signaling vias, shorting vias in the neighborhood to reduce coupling and also many other idle vias on the PCB.

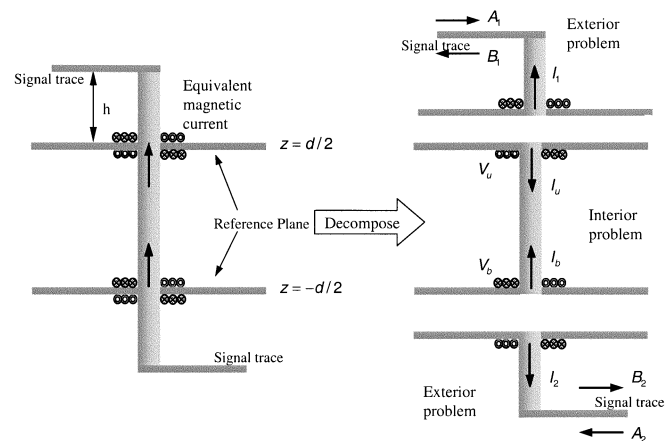


Fig. 2. Decomposition of vertical via structure.

approach [3]–[5] or empirical formulas [6]. A circularly symmetric via has been modeled using a quasi-static approach [7]. More recently, a method of moments (MoM) full-wave analysis has been applied to through-hole via geometry [8], [9]. The vertical via structure in multilayered geometry has been analyzed using equivalent circuit and microwave network analysis [10]. An attempt to account for coupling noise between coupled vias is shown in [11]. The electromagnetic coupling between two adjacent vias in a multilayered IC was analyzed by means of equivalent magnetic frill array models [11], [12] incorporated with the even- and odd-mode approach. Also, a differential via pair has been analyzed in [13]. Some of the above analysis are only for low frequency. Some are only for through-hole vias instead of vias in a multilayered structure. Some are only for two-via coupling and some analysis needs special feed-in assumption and a symmetric structure.

In this paper, we analyze the vertical via structure in layered geometry. A typical multivia structure is shown in Fig. 1. Using the equivalence principle, a vertical via structure is decomposed into an interior and an exterior problem (Fig. 2).

The interior problem consists of magnetic sources between plane conductors and vias as well as cylindrical via structures. Recently we solved the interior problem of several hundred vias using Foldy–Lax equations in vector cylindrical waves and waveguide modes [14]. The solution of Foldy–Lax equations was computed by matrix inversion. The exterior problem was modeled by a transmission line with a characteristic impedance. In this paper, we make the following major extensions and improvement of the previous method.

- 1) The exterior transmission line is modeled by bent wires using the MoM approach, thus including the effect of reflection in the exterior problem. We further extend the MoM approach of single bent wire in [8], [9] and consider coupled bent wires in the exterior problem.
- 2) The case of multilayered geometry is considered.
- 3) To facilitate the solution of the case of several thousand vias, the equations for the exterior problem are combined with the Foldy–Lax equation for the interior problem to form a single system of equations with the incident and reflected wave amplitudes as unknowns.
- 4) Numerical results are illustrated for common-mode and differential-mode signaling with idle and shorting vias.

Section II of the paper gives the formulation of the interior problem, which includes the vector cylindrical wave expansion [15] of the Green's function of a cylindrical scatterer between two parallel PECs and the multiple scattering formula using Foldy–Lax equations. Given the voltage at the via aperture, a magnetic frill current is used as an equivalent source. The magnetic frill current excites cylindrical waves of magnetic field inside the parallel plate waveguide. The port currents are expressed in terms of the solutions of the Foldy–Lax equations. An admittance matrix is given for a single via. A simple analytic formula in the short via limit is also derived. In Section III, we extend the MoM approach of [8] to treat the exterior problem of coupled wires bent into vertical vias outside the parallel plate waveguide. In Section IV, matrix equations are derived to represent the combined exterior and interior problem. An iterative method is applied to calculate the solution. In Section V, numerical results of the scattering parameters and loss are illustrated for a large frequency range and for various multilayered via configurations. We also illustrate results for cases with thousands of vias in differential signaling.

II. FORMULATION: INTERIOR

A. Single Via

A single vertical via is decomposed into interior and exterior problems as in Fig. 2 using equivalent magnetic sources at the apertures. The via cylinders are modeled as conducting cylindrical scatterers between two PECs. A cylindrical wave expansion of a dyadic Green's function of a cylindrical scatterer in terms of waveguide modes is used. Based upon the Green's function, we excite the structure using a voltage source at the port, which is equivalent to a magnetic current ring source at

the via aperture. The electric currents are then found on the surface of via cylinders. The admittance matrix of the via is then obtained which fully describes the interior structure of a vertical via.

1) *Cylindrical Wave Expansion of a Dyadic Green's Function Between Two PECs:* Consider two perfect electric conductors at $z = d/2$ and $z = -d/2$ (Fig. 2). Let the magnetic current source be at z' that is between the two PECs and flow in the horizontal plane. Then the Green's function is

$$\overline{\overline{G}} = \overline{\overline{G}}_P + \overline{\overline{G}}_R \quad (1)$$

where $\overline{\overline{G}}_P$ and $\overline{\overline{G}}_R$ are the primary Green's function and the response Green's function, respectively. The Green's function of two parallel PECs [16], [17] will be the primary field for this case as the source between two parallel plates generates the incident field onto the cylinder scatterer. In the following, we use the upper sign for $z < z'$, the lower sign for $z > z'$, and $\overline{\overline{I}}_t = \hat{x}\hat{x} + \hat{y}\hat{y}$ is the transverse dyad.

For $\rho < \rho'$, we have

$$\begin{aligned} & \overline{\overline{G}}_P(\overline{\mathbf{r}}, \overline{\mathbf{r}}') \cdot \overline{\overline{I}}_t \\ &= -\frac{\eta}{4d} \sum_{n,\ell} \frac{(-1)^{n+\ell}}{k_{\rho\ell}^2} f_\ell \left(1 + e^{2jk_{z\ell}(z' \mp d/2)} \right) \\ & \quad \cdot e^{-jk_{z\ell}(z' \mp d/2)} Rg\overline{\overline{H}}_n^{\text{TM}}(k_{\rho\ell}, k_{z\ell}, \overline{\rho}, z \pm d/2) \\ & \quad \cdot \overline{\overline{m}}_{-n}(k_{\rho\ell}, k_{z\ell}, \overline{\rho}') e^{jn\phi'} \cdot \overline{\overline{I}}_t \\ & \quad + \frac{j\eta}{4d} \sum_{n,\ell} \frac{(-1)^{n+\ell}}{k_{\rho\ell}^2} f_\ell \left(1 + e^{2jk_{z\ell}(z' \mp d/2)} \right) \\ & \quad \cdot e^{-jk_{z\ell}(z' \mp d/2)} Rg\overline{\overline{H}}_n^{\text{TE}}(k_{\rho\ell}, k_{z\ell}, \overline{\rho}, z \pm d/2) \\ & \quad \cdot \overline{\overline{n}}_{-n}(k_{\rho\ell}, k_{z\ell}, \overline{\rho}') e^{jn\phi'} \cdot \overline{\overline{I}}_t \end{aligned} \quad (2)$$

where $f_\ell = 1/2$ for $\ell = 0$, $f_\ell = 1$ for $\ell = 1, 2, \dots$, $\eta = \sqrt{\mu/\epsilon}$ is the wave impedance, and $k_{z\ell} = l\pi/d$, $l = 0, 1, 2, \dots$. For $\rho > \rho'$, $\overline{\overline{G}}_P(\overline{\mathbf{r}}, \overline{\mathbf{r}}') \cdot \overline{\overline{I}}_t$ can be obtained by symmetry.

The magnetic modal solutions are defined in [14]. The summation of the modal solutions starts with $\ell = 0$ for TM waves and starts with $\ell = 1$ for TE waves, and summation of harmonics are for $n = -\infty$ to ∞ .

2) *Dyadic Green's Function of a Cylindrical Scatterer Between Two PECs:* To include vertical vias into this structure, we model the vertical vias as conducting cylindrical scatterers and derive the Green's function of a conducting cylindrical scatterer between two parallel PECs.

Consider a perfectly conducting cylinder placed between two parallel plates at $z = d/2$ and $z = -d/2$. The cylinder is of radius a and is centered at $\overline{\rho} = 0$. Then $\overline{\overline{G}}_R$ is the Green's function accounting for the scattering by the cylinder. For a response Green's function, the regular TM mode, $Rg\overline{\overline{H}}_n^{\text{TM}}$, has a scattering coefficient of $T_n^{(N)}$ for scattering by a cylinder, while the regular TE mode, $Rg\overline{\overline{H}}_n^{\text{TE}}$, has a scattering coefficient of $T_n^{(M)}$.

In the following, we use the upper sign for source at $z' = d/2$ and a lower sign for source at $z' = -d/2$ as

$$\begin{aligned} & \overline{\mathbf{G}}_R(\overline{\rho}, \overline{\rho}') \cdot \overline{\mathbf{I}}_t \\ &= -\frac{\eta}{2d} \sum_{n,\ell} \frac{(-1)^{n+\ell}}{k_{\rho\ell}^2} f_\ell T_n^{(N)} \overline{\mathbf{H}}_n^{\text{TM}}(k_{\rho\ell}, k_{z\ell}, \overline{\rho}, z \pm d/2) \\ & \quad \cdot \overline{\mathbf{m}}_{-n}(k_{\rho\ell}, k_{z\ell}, \overline{\rho}') e^{jn\phi'} \cdot \overline{\mathbf{I}}_t \\ & \quad + \frac{j\eta}{2d} \sum_{n,\ell} \frac{(-1)^{n+\ell}}{k_{\rho\ell}^2} f_\ell T_n^{(M)} \overline{\mathbf{H}}_n^{\text{TE}}(k_{\rho\ell}, k_{z\ell}, \overline{\rho}, z \pm d/2) \\ & \quad \cdot \overline{\mathbf{n}}_{-n}(k_{\rho\ell}, k_{z\ell}, \overline{\rho}') e^{jn\phi'} \cdot \overline{\mathbf{I}}_t \end{aligned} \quad (3)$$

where the T -matrix scattering coefficients are $T_n^{(M)} = -(J_n'(k_{\rho\ell}a)/H_n^{(2)'}(k_{\rho\ell}a))$ and $T_n^{(N)} = -(J_n(k_{\rho\ell}a)/H_n^{(2)}(k_{\rho\ell}a))$.

3) *Magnetic Field and Surface Current Density on the Cylinder*: Let the source be located with $\rho' > a$. The surface current density on the cylinder is

$$\begin{aligned} \overline{\mathbf{J}}_s &= \frac{jk}{2d} \sum_{n,\ell} \frac{(-1)^{n+\ell}}{k_{\rho\ell}^2} f_\ell \overline{\mathbf{J}}_{sn}^{\text{TM}}(k_\rho, k_z, z \pm d/2) \\ & \quad \cdot \int d\overline{\rho}' \overline{\mathbf{m}}_{-n}(k_{\rho\ell}, k_{z\ell}, \overline{\rho}') e^{jn\phi'_{\overline{\rho}'}} \cdot \overline{\mathbf{M}}_s(\overline{\rho}') \\ & \quad + \frac{k}{2d} \sum_{n,\ell} \frac{(-1)^{n+\ell}}{k_{\rho\ell}^2} f_\ell \overline{\mathbf{J}}_{sn}^{\text{TE}}(k_\rho, k_z, z \pm d/2) \\ & \quad \cdot \int d\overline{\rho}' \overline{\mathbf{n}}_{-n}(k_{\rho\ell}, k_{z\ell}, \overline{\rho}') e^{jn\phi'_{\overline{\rho}'}} \cdot \overline{\mathbf{M}}_s(\overline{\rho}') \end{aligned} \quad (4)$$

where the modal solutions of surface current density $\overline{\mathbf{J}}_{sn}^{\text{TE}}(k_\rho, k_z, z)$ and $\overline{\mathbf{J}}_{sn}^{\text{TM}}(k_\rho, k_z, z)$ are defined in [14].

4) *Admittance Matrix of a Single Via*: To obtain the admittance matrix of a single via, we excite the structure using voltage sources of magnetic frill and solve for the magnetic field. The surface current on the cylinder can be calculated from the magnetic field.

The current on the surface of the cylinder in the positive z direction is

$$\begin{aligned} I_s &= \int_0^{2\pi} a \overline{\mathbf{J}}_s \cdot \hat{\mathbf{z}} d\phi \\ &= -\frac{jk}{\eta d} \frac{4\pi V}{\ln \frac{b}{a}} \sum_\ell \frac{(-1)^\ell}{k_{\rho\ell}^2} f_\ell \frac{1}{H_0^{(2)}(k_{\rho\ell}a)} \\ & \quad \cdot \{\cos k_{z\ell}(z \pm d/2)\} \left[H_0^{(2)}(k_{\rho\ell}b) - H_0^{(2)}(k_{\rho\ell}a) \right]. \end{aligned} \quad (5)$$

The admittance matrix elements are then

$$Y_{11} = \frac{4\pi\omega\epsilon j}{d \ln \frac{b}{a}} \sum_l \frac{f_l}{k_{\rho\ell}^2} \left[\frac{H_0^{(2)}(k_{\rho\ell}b)}{H_0^{(2)}(k_{\rho\ell}a)} - 1 \right] \quad (6)$$

$$Y_{12} = -\frac{4\pi\omega\epsilon j}{d \ln \frac{b}{a}} \sum_l \frac{(-1)^l f_l}{k_{\rho\ell}^2} \left[\frac{H_0^{(2)}(k_{\rho\ell}b)}{H_0^{(2)}(k_{\rho\ell}a)} - 1 \right] \quad (7)$$

and due to symmetry we have $Y_{21} = Y_{12}$ and $Y_{22} = Y_{11}$.

5) *Analytic Formulas for Short Vias*: For the case of short vias when the layer thickness is small ($kd \ll 1$), note that d is the layer thickness and not the via length as there are sections of the via outside the layered structure. The section of the via outside the layers is included in the exterior problem. If we assume that the via radius and via aperture are small ($ka \ll 1$, $kb \ll 1$), then we retain only the $\ell = 0$ term in the expressions. Using a small argument approximation for the Hankel function, we have

$$\begin{aligned} Y_{11} &= Y_{22} \\ &= -Y_{12} \\ &= -Y_{21} \\ &= -\frac{2\pi j}{\omega\mu d \left[-\log\left(\frac{\alpha ka}{2}\right) - j\frac{\pi}{2} \right]} \end{aligned} \quad (8)$$

where $\alpha = 1.781$. This can be expressed in terms of a simple series impedance for the via of

$$Z = j\omega \frac{\mu d}{2\pi} \left[-\log\left(\frac{\alpha ka}{2}\right) - j\frac{\pi}{2} \right] = j\omega L + R. \quad (9)$$

Note that the inductance L has an $\omega \log \omega$ dependence while the resistance R is linear with ω . The capacitance will be included if we include higher order modes of $l > 0$.

For the case of a multilayered via, if the total length of the entire via through all the layers is still small, then the above expression is still valid with d replaced by the sum of the lengths of the different layers. This means that d corresponds to the total length of the via inside the layers. Results of the simple formula have been compared to the exact analysis and are in good agreement in the short via limit.

B. Multivia

1) *Multiple Scattering Among Vias*: For multivia coupling, we consider coupling among all the vias. Consider two perfect electric conductors at $z = d/2$ and $z = -d/2$. In the multiple-via coupling problem, the equivalence principle is invoked with equivalent magnetic sources at $z' = \pm d/2$. Consider N via cylinders between the two parallel plates centered at $\overline{\rho}_1, \overline{\rho}_2, \dots, \overline{\rho}_N$ and magnetic surface current density $\overline{\mathbf{M}}_s = \overline{\mathbf{M}}_{su}$ at $(\overline{\rho}', z' = d/2)$ and $\overline{\mathbf{M}}_s = \overline{\mathbf{M}}_{sb}$ at $(\overline{\rho}', z' = -d/2)$.

2) *Excitation of Magnetic Frill Current*: Let there be magnetic frill currents at the aperture of via j , $j = 1, 2, 3, \dots, N$. At $z' = d/2$, we have

$$\overline{\mathbf{M}}_{su}(\overline{\rho}') = -\frac{V_{ju}}{|\overline{\rho}' - \overline{\rho}_j| \ln \frac{b}{a}} \hat{\phi}'_{\rho\rho_j}, \quad \text{for } a \leq |\overline{\rho}' - \overline{\rho}_j| \leq b \quad (10)$$

and at $z' = -d/2$ we have

$$\overline{\mathbf{M}}_{sb}(\overline{\rho}') = -\frac{V_{jb}}{|\overline{\rho}' - \overline{\rho}_j| \ln \frac{b}{a}} \hat{\phi}'_{\rho\rho_j}, \quad \text{for } a \leq |\overline{\rho}' - \overline{\rho}_j| \leq b. \quad (11)$$

With these sources, only TM modes are excited. After multiple scattering, the final exciting field of cylinder p is

$$\overline{\mathbf{H}}_{ex}^{(p)} = \sum_{m,\ell} w_{\ell m}^{\text{TM}(p)} R_g \overline{\mathbf{H}}_m^{\text{TM}}(k_{\rho\ell}, k_{z\ell}, \overline{\rho} - \overline{\rho}_p, z \pm d/2) \quad (12)$$

where $w_{\ell m}^{\text{TM}(p)}$ is exciting field coefficients.

The Foldy–Lax multiple scattering equations are in the following form [17]:

$$w_{\ell n}^{\text{TM}(q)} = a_{\ell n}^{\text{TM}(q)} + \sum_{\substack{p=1 \\ p \neq q}}^N \sum_{m=-\infty}^{\infty} H_{n-m}^{(2)} \cdot (k_{\rho\ell} |\bar{\rho}_p - \bar{\rho}_q|) e^{j(n-m)\phi_{\bar{\rho}_p \bar{\rho}_q}} T_m^{(N)} w_{\ell m}^{\text{TM}(p)} \quad (13)$$

where $a_{\ell n}^{\text{TM}(q)}$ is the incident field of the current source onto cylinder q . In the Foldy–Lax equation there is no coupling between different ℓ 's because each ℓ corresponds to a specific $k_{z\ell}$.

We solve Foldy–Lax equations for $w_{\ell n}^{\text{TM}(q)}$ and find current I^{uu} on the cylinders, which is current at $z = d/2$ due to source at $z' = d/2$. Similarly we find current I^{bu} , which is current at $z = -d/2$ due to the source at $z' = d/2$. The cases with sources at $z' = -d/2$ can be done similarly, giving currents I^{ub} and I^{bb} .

3) *Matrix Notation for the Interior Problem:* Suppose we have N vias, and we keep to $\ell = L_{\max}$ and multipoles up to $n = \pm N_{\max}$. Then the dimension of \bar{w}_ℓ is $(2N_{\max} + 1) \times N$. Using a combined index β of cylinder index $q = 1, 2, \dots, N$ and multipole index $n = -N_{\max}, -N_{\max} + 1, \dots, 0, 1, N_{\max}$, we have $\beta(q, n) = (2N_{\max} + 1) \times (q - 1) + n + N_{\max} + 1$. Thus, $\beta = 1, 2, \dots, M$ where $M = N \times (2N_{\max} + 1)$. Let superscript T denote the transpose of matrix

$$\bar{w}_\ell^T = \begin{bmatrix} w_{\ell(-N_{\max})}^{(1)} & w_{\ell(-N_{\max}+1)}^{(1)} & \cdots & w_{\ell(N_{\max})}^{(1)} \\ w_{\ell(-N_{\max})}^{(2)} & \cdots & w_{\ell(N_{\max})}^{(2)} & \cdots \cdots w_{\ell(N_{\max})}^{(N)} \end{bmatrix}. \quad (14)$$

The Foldy–Lax matrix \bar{F}_ℓ is of dimension $N(2N_{\max} + 1) \times N(2N_{\max} + 1) = M \times M$

$$\left[\bar{F}_\ell \right]_{qn, pm} = \delta_{nm} \delta_{qp} - (1 - \delta_{pq}) H_{n-m}^{(2)} (k_{\rho\ell} |\bar{\rho}_p - \bar{\rho}_q|) \cdot e^{j(n-m)\phi_{\bar{\rho}_p \bar{\rho}_q}} T_m^{(N)} \quad (15)$$

where q and p are cylinder indices and n and m are multipole indices.

Define \bar{E}_ℓ to have dimensions $M \times N$ to represent the incident field coefficients

$$\left(\bar{E}_\ell \right)_{qm, p} = [\bar{a}_{\ell p}]_{qm}. \quad (16)$$

For the case of magnetic current sources

$$\begin{aligned} [\bar{a}_{\ell p}]_{qm} &= \frac{jk}{2d} \frac{(-1)^\ell}{k_{\rho\ell}^2} f_\ell \frac{2\pi}{\ln \frac{b}{a}} \delta_{n0} \\ &\cdot \left[H_0^{(2)}(k_{\rho\ell} b) - H_0^{(2)}(k_{\rho\ell} a) \right], \quad \text{if } q = p \\ &= \frac{jk}{2d} \frac{(-1)^{n+\ell}}{k_{\rho\ell}^2} f_\ell H_n^{(2)}(k_{\rho\ell} |\bar{\rho}_q - \bar{\rho}_p|) e^{jn\phi_{\bar{\rho}_q \bar{\rho}_p}} \\ &\cdot \left[\frac{2\pi}{\ln \frac{b}{a}} [J_0(k_{\rho\ell} b) - J_0(k_{\rho\ell} a)] \right], \quad \text{if } q \neq p. \end{aligned} \quad (17)$$

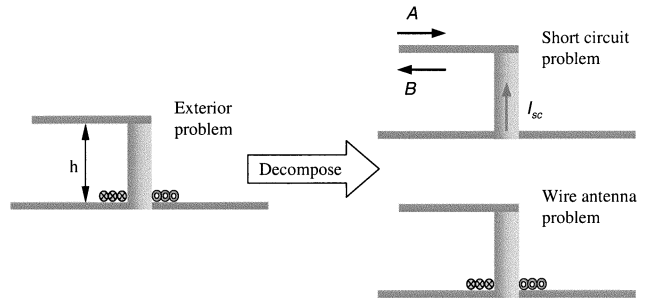


Fig. 3. Decomposition of the exterior problem.

For voltage sources at upper aperture $z' = d/2$, let the voltage vector \bar{V}^u be of dimension N , with $(\bar{V}^u)_j = V_{ju}$. In matrix form, the Foldy–Lax equation is

$$\bar{F}_\ell \bar{w}_\ell^{(u)} = \bar{E}_\ell \bar{V}^u. \quad (18)$$

Solving (18), we have current on the p th cylinder at the upper aperture \bar{I}^{uu} and current at the lower aperture \bar{I}^{bu} given by

$$I^{(p)uu} = \sum_\ell B_\ell w_{\ell 0}^{\text{TM}(p)u} \quad (19)$$

$$I^{(p)bu} = \sum_\ell D_\ell w_{\ell 0}^{\text{TM}(p)u} \quad (20)$$

where

$$B_\ell = \frac{4(-1)^\ell}{\eta H_0^{(2)}(k_{\rho\ell} a)} \quad (21)$$

$$D_\ell = \frac{4}{\eta H_0^{(2)}(k_{\rho\ell} a)}. \quad (22)$$

Similarly, we have for voltage sources at lower aperture $z' = -d/2$,

$$\bar{F}_\ell \bar{w}_\ell^{(b)} = \bar{E}_\ell \bar{V}^b \quad (23)$$

$$I^{(p)ub} = \sum_\ell B_\ell w_{\ell 0}^{\text{TM}(p)b} \quad (24)$$

$$I^{(p)bb} = \sum_\ell D_\ell w_{\ell 0}^{\text{TM}(p)b}. \quad (25)$$

The port current is the sum of current due to upper and bottom sources

$$I^{(p)u} = I^{(p)uu} + I^{(p)ub} \quad (26)$$

$$I^{(p)b} = I^{(p)bu} + I^{(p)bb}. \quad (27)$$

III. EXTERIOR PROBLEM

The exterior problem consists of a transmission line of bent wire. For a single via, we solve the exterior problem using the MoM technique following [8], [9] (Fig. 3). In Fig. 3, the exterior problem is decomposed into a short-circuit problem and wire antenna problem. For the wire antenna problem, let Y_{ant} be the input admittance of the wire antenna, and T_{ant} be the amplitude of the excited TEM mode in wire antenna with a unit voltage across the aperture. For the short-circuit problem, let Γ_{sc} be the reflection coefficient of the short-circuit problem, and I_{sc} be the

current at the short-circuit end when the structure is excited with a unit TEM wave incidence. The quantities A and B are the incident and reflected TEM waves at the port, and V and I are the port voltage and current at the aperture.

In general, the exterior problem of a multiview structure can consist of large number of transmission lines that are bent to connect to the sections of vias that are outside the parallel plate waveguide. In this paper, we consider two types of exterior problem.

1) *Case A—Exterior Problem With Uncoupled Transmission Lines:* In this case, there are N transmission lines/bent wires above the parallel plate waveguide that are uncoupled and N transmission lines/wires below the parallel plate waveguide that are also uncoupled. For simplicity, we shall assume that the transmission lines are identical. The exterior problem has the matrix equation as follows. For the p th via, we have

$$\begin{bmatrix} B_u^{(p)} \\ I_u^{(p)} \end{bmatrix} = \begin{bmatrix} \Gamma_{sc} & T_{ant} \\ I_{sc} & Y_{ant} \end{bmatrix} \begin{bmatrix} A_u^{(p)} \\ -V_u^{(p)} \end{bmatrix} \quad (28)$$

$$\begin{bmatrix} B_b^{(p)} \\ -I_b^{(p)} \end{bmatrix} = \begin{bmatrix} \Gamma_{sc} & T_{ant} \\ I_{sc} & Y_{ant} \end{bmatrix} \begin{bmatrix} A_b^{(p)} \\ V_b^{(p)} \end{bmatrix} \quad (29)$$

for the upper port and the bottom port, respectively.

2) *Case B—Coupling Among a Small Number of Lines/Wires in the Exterior Problem:* We next consider the case where the exterior transmission lines are only coupled to their nearest neighbors. Then the exterior problem of many lines will be decomposed into block matrices. In this paper, we consider the case of two coupled transmission lines that are bent into the two vertical via sections outside the parallel plate waveguide (Fig. 4). Thus, the exterior problem of many lines consists of sets of two coupled lines and uncoupled lines. (The method can be readily extended to coupling among a finite number of lines.) We extend the MoM approach in [8], [9] to consider the case of coupled bent wires. Let lines 1 and 2 be the two coupled lines/bent wires. Then we have

$$\begin{bmatrix} B_u^{(1)} \\ B_u^{(2)} \\ I_u^{(1)} \\ I_u^{(2)} \end{bmatrix} = \begin{bmatrix} \Gamma_{sc11} & \Gamma_{sc12} & T_{ant11} & T_{ant12} \\ \Gamma_{sc21} & \Gamma_{sc22} & T_{ant21} & T_{ant22} \\ I_{sc11} & I_{sc12} & Y_{ant22} & Y_{ant22} \\ I_{sc21} & I_{sc22} & Y_{ant22} & Y_{ant22} \end{bmatrix} \begin{bmatrix} A_u^{(1)} \\ A_u^{(2)} \\ -V_u^{(1)} \\ -V_u^{(2)} \end{bmatrix} \quad (30)$$

$$\begin{bmatrix} B_b^{(1)} \\ B_b^{(2)} \\ -I_b^{(1)} \\ -I_b^{(2)} \end{bmatrix} = \begin{bmatrix} \Gamma_{sc11} & \Gamma_{sc12} & T_{ant11} & T_{ant12} \\ \Gamma_{sc21} & \Gamma_{sc22} & T_{ant21} & T_{ant22} \\ I_{sc11} & I_{sc12} & Y_{ant22} & Y_{ant22} \\ I_{sc21} & I_{sc22} & Y_{ant22} & Y_{ant22} \end{bmatrix} \begin{bmatrix} A_b^{(1)} \\ A_b^{(2)} \\ V_b^{(1)} \\ V_b^{(2)} \end{bmatrix} \quad (31)$$

Using the equivalence principle and the image theory, the two coupled transmission lines shown in the left of Fig. 4 can be treated as the new structure shown in the right of Fig. 4. We extend the approach in [8]. Let the two transmission lines be thin wire so that the current density on them can be represented

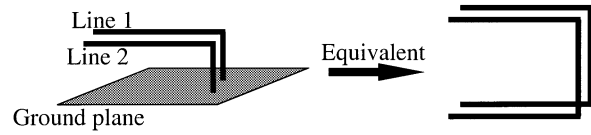


Fig. 4. Coupled exterior structure.

by $I_1(s)$ and $I_2(s)$. The integral equation that the currents have to obey is

$$j\omega\epsilon \hat{s} \cdot \bar{E}^i(s) = \int I_1(s') \left[\frac{\partial^2}{\partial s \partial s'} - k^2 \hat{s} \cdot \hat{s}' \right] G(s, s') ds' + \int I_2(s') \left[\frac{\partial^2}{\partial s \partial s'} - k^2 \hat{s} \cdot \hat{s}' \right] G(s, s') ds' \quad (32)$$

where s is the point on the two transmission lines and \hat{s} is the unit vector tangential to the transmission line at the point of s . $G(s, s') = e^{-jkR}/4\pi R$ is the Green's function of free space where $R = |\bar{s} - \bar{s}'|$. The incident field $\bar{E}^i(s)$ on the wire is determined by the frill magnetic current

$$\bar{E}^i(s) = \nabla \times \left\{ \int 2 \cdot G(s, \bar{r}') \overline{M}_1(\bar{r}') d\Omega' + \int 2 \cdot G(s, \bar{r}') \overline{M}_2(\bar{r}') d\Omega' \right\} \quad (33)$$

Equation (32) can be solved using the method of moment [19]. Using the triangle basis function, current $I_1(s)$ and $I_2(s)$ can be expressed as

$$I_1(s) = \sum_{n=0}^{2N} c_n^1 f_n(s) \quad (34)$$

$$I_2(s) = \sum_{n=0}^{2N} c_n^2 f_n(s). \quad (35)$$

Substituting the above equations into integral equation (32) and using Galerkin's method, we have

$$\sum_{n=1}^{N-1} \left(Z_{m,n}^{(i)(1)} + Z_{m,2N-n}^{(i)(1)} \right) c_n^1 + Z_{m,N}^{(i)(1)} c_N^1 + \sum_{n=1}^{N-1} \left(Z_{m,n}^{(i)(2)} + Z_{m,2N-n}^{(i)(2)} \right) c_n^2 + Z_{m,N}^{(i)(2)} c_N^2 = V_m^{(i)} - \left(Z_{m,0}^{(i)(1)} + Z_{m,2N}^{(i)(1)} \right) c_0^1 - \left(Z_{m,0}^{(i)(2)} + Z_{m,2N}^{(i)(2)} \right) c_0^2. \quad (36)$$

The index of $i = 1$ means the testing point is on wire 1 and $i = 2$ on wire 2. In (36), the impedance matrix elements are

$$Z_{m,n}^{(i)(j)} = \iint f_m(s^{(i)}) f_n(s'^{(j)}) \left[\frac{\partial^2}{\partial s^{(i)} \partial s'^{(j)}} - k^2 \hat{s}^{(i)} \cdot \hat{s}'^{(j)} \right] \cdot G(s^{(i)}, s'^{(j)}) ds'^{(j)} ds^{(i)} \quad (37)$$

and the column vector elements are

$$V_m^{(i)} = j\omega\epsilon \int f_m(s^{(i)}) \hat{s}^{(i)} \cdot \bar{E}^i(s^{(i)}) ds^{(i)}. \quad (38)$$

We solve matrix equation (36) and find the current distribution on the two wires. Using the matrix pencil method [18], the am-

plitudes A and B of the incident and reflected wave on the two wires can be extracted from the current distribution.

Let the voltage drop V between the via and ground plane be zero and enforce a current source such that $c_0^1 = 1$ at the truncated end of the first transmission line. The amplitudes A_1 , A_2 , B_1 , and B_2 are calculated as discussed above. Then Γ_{sc} and I_{sc} are given by

$$\Gamma_{sc11} = \frac{A_1 B_1 - A_2 B_2}{A_1 A_1 - A_2 A_2} \quad (39)$$

$$\Gamma_{sc12} = \frac{A_1 B_2 - A_2 B_1}{A_1 A_1 - A_2 A_2} \quad (40)$$

$$I_{sc11} = \frac{A_1 I_1 - A_2 I_2}{A_1 A_1 - A_2 A_2} \quad (41)$$

$$I_{sc12} = \frac{A_1 I_2 - A_2 I_1}{A_1 A_1 - A_2 A_2}. \quad (42)$$

Next let $V_u^{(1)} = -1$, $V_u^{(2)} = 0$, $c_0^1 = c_0^2 = 0$. Then the T_{ant} 's and Y_{ant} 's are given by

$$T_{ant11} = B_1 - \Gamma_{sc11} A_1 - \Gamma_{sc12} A_2 \quad (43)$$

$$T_{ant12} = B_2 - \Gamma_{sc21} A_1 - \Gamma_{sc22} A_2 \quad (44)$$

$$Y_{ant11} = I_1 - I_{sc11} A_1 - I_{sc12} A_2 \quad (45)$$

$$Y_{ant12} = I_2 - I_{sc21} A_1 - I_{sc22} A_2. \quad (46)$$

The above method illustrates the case for two coupled lines that are bent to connect to the vias outside the parallel plate waveguide. For N lines/bent wires in the exterior problem, we have

$$\bar{B}^u = \bar{\Gamma}_{sc} \bar{A}^u - \bar{T}_{ant} \bar{V}^u \quad (47)$$

$$\bar{I}^u = \bar{I}_{sc} \bar{A}^u - \bar{Y}_{ant} \bar{V}^u \quad (48)$$

$$\bar{B}^b = \bar{\Gamma}_{sc} \bar{A}^b + \bar{T}_{ant} \bar{V}^b \quad (49)$$

$$-\bar{I}^b = \bar{I}_{sc} \bar{A}^b + \bar{Y}_{ant} \bar{V}^b. \quad (50)$$

We assume that coupling only exists among a small number of lines/wires where the rest are uncoupled. Then $\bar{\Gamma}_{sc}$, \bar{T}_{ant} , \bar{I}_{sc} , and \bar{Y}_{ant} are $N \times N$ sparse matrices in block form with no coupling among the blocks. For example, if only two lines are coupled, then we have a 2×2 block and the rest of the $N \times N$ matrices are diagonal.

IV. THE COMBINATION OF INTERIOR AND EXTERIOR PROBLEMS

The combination of the results of the interior and exterior structure is carried out by relating the port voltage and current.

For a single via in single-layered geometry, let $A_1 = 1$ and $A_2 = 0$, and then we have the following matrix equation for the entire via structure:

$$\begin{bmatrix} 1 & 0 & -T_{ant1} & 0 & 0 & 0 \\ 0 & 1 & -Y_{ant1} & 0 & 0 & 0 \\ 0 & 0 & 0 & 1 & 0 & -T_{ant2} \\ 0 & 0 & 0 & 0 & 1 & -Y_{ant2} \\ 0 & 1 & Y_{11} & 0 & 0 & Y_{12} \\ 0 & 0 & Y_{21} & 0 & 1 & Y_{22} \end{bmatrix} \begin{bmatrix} B_1 \\ I_1 \\ V_1 \\ B_2 \\ I_2 \\ V_2 \end{bmatrix} = \begin{bmatrix} \Gamma_{sc1} \\ I_{sc1} \\ 0 \\ 0 \\ 0 \\ 0 \end{bmatrix}. \quad (51)$$

We solve (51) to get the reflected wave B_1 at port 1 and transmitted wave B_2 at port 2. Then the scattering parameters are given by

$$S_{11} = B_1/A_1 = B_1 \quad (52)$$

$$S_{12} = B_2/A_1 = B_2. \quad (53)$$

For a symmetric structure, $S_{21} = S_{12}$ and $S_{22} = S_{11}$. For an asymmetric structure, S_{21} and S_{22} can be obtained by exciting the structure at port 2 instead of port 1.

For multilayered geometry, we cascade the single-layer structure using a transfer matrix. After the cascading of transfer matrices, the result transfer matrix is then converted back to Y matrix and we use (51) and (52) to calculate the scattering matrix.

A. Multivia

In this paper, we consider two coupled bent transmission lines and the rest of the $N - 2$ lines are uncoupled for the exterior problem. However, the N vias are coupled in the interior problem.

In the previous paper [14], we solved the interior problem of the Foldy–Lax equation by matrix inversion to calculate the exciting field coefficients w_{in} . Next these are used to calculate the magnetic fields and currents which are related to port voltages. The relation between the currents and voltages in the interior problem are then substituted into the exterior problem matrix equation to find the relation between incident and reflected wave amplitudes of the transmission line. The previous method is not suitable for the case of several thousand vias or more. In this paper, to make the algorithm applicable for thousands or more vias, we combine the interior and exterior equation into a single set of matrix equations so that iterative method can be used for the resulting matrix equation.

In the interior problem, for the $\ell = 0$ mode, we include coupling of all the vias. For small layer thickness, the higher order modes are evanescent. Thus, the higher order modes are coupled in the near field only. In the simulations, we include coupling of the higher order modes ($\ell \geq 1$) for the several vias that have coupling in the corresponding exterior problem. For the $\ell = 0$ mode, including all N vias, we have

$$\bar{F}_0 \bar{W}^{(0)u} = \bar{E}_0 \bar{V}^u \quad (54)$$

$$\bar{F}_0 \bar{W}^{(0)b} = \bar{E}_0 \bar{V}^b \quad (55)$$

where \bar{F}_0 and \bar{E}_0 are dense $N \times N$ full matrices. For $\ell \geq 1$, we have

$$\bar{F}_\ell \bar{W}^{(\ell)u} = \bar{E}_\ell \bar{V}^u \quad (56)$$

$$\bar{F}_\ell \bar{W}^{(\ell)b} = \bar{E}_\ell \bar{V}^b \quad (57)$$

where \bar{F}_ℓ and \bar{E}_ℓ are given in (15) and (16). The elements in \bar{F}_ℓ and \bar{E}_ℓ are zero if the corresponding lines in the exterior problem are not coupled. Thus, for higher order modes ($\ell \geq 1$), we have block sparse matrices of \bar{F}_ℓ and \bar{E}_ℓ . Letting $\bar{P}_\ell = \bar{F}_\ell^{-1} \bar{E}_\ell$, we have

$$\bar{W}^{(\ell)u} = \bar{P}_\ell \bar{V}^u \quad (58)$$

$$\bar{W}^{(\ell)b} = \bar{P}_\ell \bar{V}^b. \quad (59)$$

Note that taking the inverse of block matrices $\bar{E}_\ell, \bar{F}_\ell, \bar{P}_\ell$ ($\ell \geq 1$), $\bar{\Gamma}_{sc}, \bar{T}_{ant}, \bar{I}_{sc}$ and \bar{Y}_{ant} are computationally inexpensive.

From the interior problem we have

$$\begin{aligned} \bar{I}^u &= \bar{I}^{uu} + \bar{I}^{ub} \\ &= \sum_{\ell=0}^{\infty} B_\ell \bar{W}^{(\ell)u} + \sum_{\ell=0}^{\infty} D_\ell \bar{W}^{(\ell)b} \\ &= B_0 \bar{W}^{(0)u} + D_0 \bar{W}^{(0)b} + \sum_{\ell=1}^{\infty} B_\ell \bar{W}^{(\ell)u} + \sum_{\ell=1}^{\infty} D_\ell \bar{W}^{(\ell)b} \\ &= B_0 \bar{W}^{(0)u} + D_0 \bar{W}^{(0)b} + \bar{Y}_{extra}^{uu} \bar{V}^u + \bar{Y}_{extra}^{ub} \bar{V}^b \end{aligned} \quad (60)$$

$$\bar{I}^b = D_0 \bar{W}^{(0)u} + B_0 \bar{W}^{(0)b} + \bar{Y}_{extra}^{bu} \bar{V}^u + \bar{Y}_{extra}^{bb} \bar{V}^b \quad (61)$$

where $\bar{Y}_{extra}^{uu}, \bar{Y}_{extra}^{uu}, \bar{Y}_{extra}^{uu}$, and \bar{Y}_{extra}^{uu} are calculated from the block matrices

$$\bar{Y}_{extra}^{uu} = \bar{Y}_{extra}^{bb} = \sum_{\ell=1}^{\infty} B_\ell \bar{P}_\ell \quad (62)$$

$$\bar{Y}_{extra}^{ub} = \bar{Y}_{extra}^{bu} = \sum_{\ell=1}^{\infty} D_\ell \bar{P}_\ell. \quad (63)$$

Note that \bar{Y}_{extra}^{uu} and \bar{Y}_{extra}^{ub} are also $N \times N$ block matrices. Since $B_0 = D_0$, we have

$$\bar{I}^u - \bar{I}^b = \left(\bar{Y}_{extra}^{uu} - \bar{Y}_{extra}^{ub} \right) (\bar{V}^u - \bar{V}^b). \quad (64)$$

From the exterior problem we have

$$\bar{V}^u = \bar{T}_{ant}^{-1} \bar{B}^u - \bar{T}_{ant}^{-1} \bar{\Gamma}_{sc} \bar{A}^u \quad (65)$$

$$\bar{V}^b = -\bar{T}_{ant}^{-1} \bar{B}^b + \bar{T}_{ant}^{-1} \bar{\Gamma}_{sc} \bar{A}^b \quad (66)$$

$$\bar{I}^u = -\bar{Y}_{ant} \bar{T}_{ant}^{-1} \bar{B}^u + \left(\bar{I}_{sc} + \bar{Y}_{ant} \bar{T}_{ant}^{-1} \bar{\Gamma}_{sc} \right) \bar{A}^u \quad (67)$$

$$\bar{I}^b = \bar{Y}_{ant} \bar{T}_{ant}^{-1} \bar{B}^b - \left(\bar{I}_{sc} + \bar{Y}_{ant} \bar{T}_{ant}^{-1} \bar{\Gamma}_{sc} \right) \bar{A}^b. \quad (68)$$

Subtracting (65) and (67), respectively, from (66) and (68) and substituting into (64), we have

$$\begin{aligned} & -\bar{Y}_{ant} \bar{T}_{ant}^{-1} (\bar{B}^u + \bar{B}^b) \\ & + \left(\bar{I}_{sc} + \bar{Y}_{ant} \bar{T}_{ant}^{-1} \bar{\Gamma}_{sc} \right) (\bar{A}^u + \bar{A}^b) \\ & = \left(\bar{Y}_{extra}^{uu} - \bar{Y}_{extra}^{ub} \right) \\ & \cdot \left[\bar{T}_{ant}^{-1} (\bar{B}^u + \bar{B}^b) - \bar{T}_{ant}^{-1} \bar{\Gamma}_{sc} (\bar{A}^u + \bar{A}^b) \right]. \end{aligned} \quad (69)$$

Hence

$$(\bar{B}^u + \bar{B}^b) = \bar{\Gamma}_{ratio} (\bar{A}^u + \bar{A}^b) \quad (70)$$

where

$$\begin{aligned} \bar{\Gamma}_{ratio} &= \bar{T}_{ant} \left[\bar{Y}_{ant} + \left(\bar{Y}_{extra}^{uu} - \bar{Y}_{extra}^{ub} \right) \right]^{-1} \\ & \cdot \left[\bar{I}_{sc} + \left(\bar{Y}_{ant} + \bar{Y}_{extra}^{uu} - \bar{Y}_{extra}^{ub} \right) \bar{T}_{ant}^{-1} \bar{\Gamma}_{sc} \right]. \end{aligned} \quad (71)$$

Note that the matrices in (71) are all block $N \times N$ matrices, so taking the inverse is not computationally expensive nor is there much requirement for the memory.

Using (70), (66) can be rewritten as

$$\begin{aligned} \bar{V}^b &= -\bar{T}_{ant}^{-1} \left[-\bar{B}^u + \bar{\Gamma}_{ratio} (\bar{A}^u + \bar{A}^b) \right] + \bar{T}_{ant}^{-1} \bar{\Gamma}_{sc} \bar{A}^b \\ &= \bar{T}_{ant}^{-1} \bar{B}^u - \bar{T}_{ant}^{-1} \bar{\Gamma}_{ratio} \bar{A}^u + \bar{T}_{ant}^{-1} \left[\bar{\Gamma}_{sc} - \bar{\Gamma}_{ratio} \right] \bar{A}^b. \end{aligned} \quad (72)$$

We multiply (60) by \bar{F}_0 . Then

$$\begin{aligned} \bar{F}_0 \bar{I}^u &= \left(B_0 \bar{E}_0 + \bar{F}_0 \bar{Y}_{extra}^{uu} \right) \cdot \bar{V}^u \\ & \quad + \left(D_0 \bar{E}_0 + \bar{F}_0 \bar{Y}_{extra}^{ub} \right) \cdot \bar{V}^b. \end{aligned} \quad (73)$$

Substituting \bar{V}^u, \bar{V}^b , and \bar{I}^u into (73), we have

$$\begin{aligned} & \left[\bar{F}_0 \left(-\bar{Y}_{ant} + \bar{Y}_{extra}^{uu} + \bar{Y}_{extra}^{ub} \right) + (B_0 + D_0) \bar{E}_0 \right] \bar{T}_{ant}^{-1} \cdot \bar{B}^u \\ & = \left[-\bar{F}_0 \left(\bar{I}_{sc} + \bar{Y}_{ant} \bar{T}_{ant}^{-1} \bar{\Gamma}_{sc} \right) - \left(B_0 \bar{E}_0 + \bar{F}_0 \bar{Y}_{extra}^{uu} \right) \bar{\Gamma}_{sc} \right. \\ & \quad \left. - \left(D_0 \bar{E}_0 + \bar{F}_0 \bar{Y}_{extra}^{ub} \right) \bar{T}_{ant}^{-1} \bar{\Gamma}_{ratio} \right] \cdot \bar{A}^u \\ & \quad + \left(D_0 \bar{E}_0 + \bar{F}_0 \bar{Y}_{extra}^{ub} \right) \bar{T}_{ant}^{-1} \left[\bar{\Gamma}_{sc} - \bar{\Gamma}_{ratio} \right] \cdot \bar{A}^b. \end{aligned} \quad (74)$$

Note that only \bar{E}_0 and \bar{F}_0 are dense full matrices in (74).

Equation (74) represents the combined matrix equation incorporating both the exterior and interior problems. It has N unknowns in column vector \bar{B}^u . It can be solved for \bar{B}^u using an iterative method. After \bar{B}^u is solved, \bar{B}^b can be obtained with (70).

V. RESULTS AND DISCUSSION

The results of our method have been compared in [20] with the single-via and coupled-via cases in [10] and [11] and are in good agreement. The computational algorithm in this paper is efficient. Simulation of 2500 vias is completed in 56 s on a PC with an AMD Athlon processor of 866 MHz and 512-Mb memory [20].

Fig. 5 shows the propagation characteristics of a through-hole via, a single-layered vertical via, and a nine-layer vertical via. The inner radius of the via is $a = 0.127$ mm, the outer radius of the via is $b = 0.381$ mm, and the layer thickness of each layer is $d = 0.254$ mm, with a layer relative dielectric constant of $\epsilon_r = 2.2$. For the exterior parameter, the wire radius is the same as the via inner radius, and the wire bend is at $h = 1.016$ mm. Fig. 6 shows the loss comparison of these three kinds of vias. The loss is defined as $L = 1 - |S_{11}|^2 - |S_{21}|^2$. Loss is due to: 1) radiation by the wire along the planar waveguide; 2) discontinuity at the wire bend and the via aperture; and 3) parallel plate waveguide modes excited between metal layers. We can see clearly that a through-hole via has the least radiation loss; a single-layered vertical via has more radiation loss because of the parallel plate waveguide effect of the interior structure. A nine-layer vertical via has the most loss among the three. Note that the layer thickness of each layer is constant. Thus, nine layers have a larger total thickness than one layer. Thus, the more layers there are, the more energy will be coupled

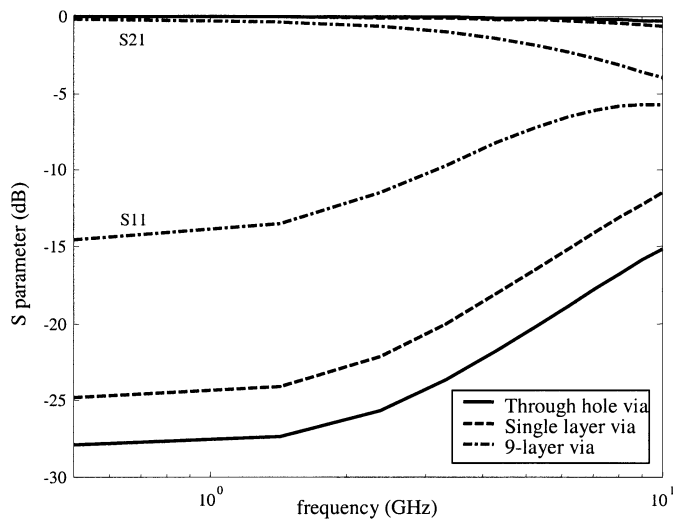
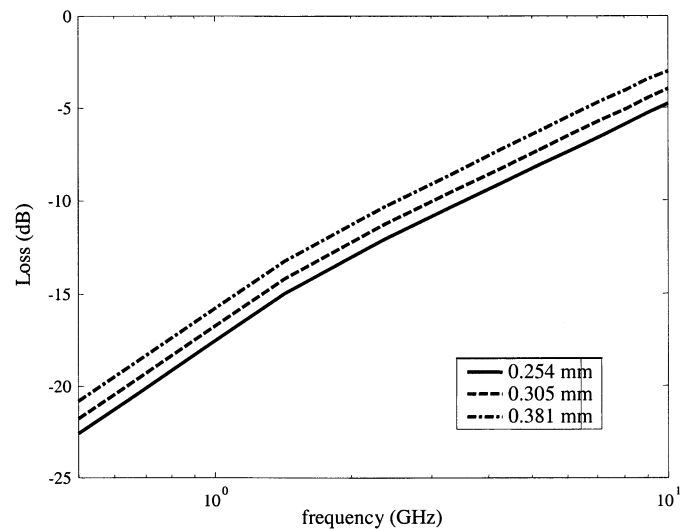

 Fig. 5. S parameters of three kinds of vias.


Fig. 7. Loss comparison of a nine-layer via with different layer thicknesses.

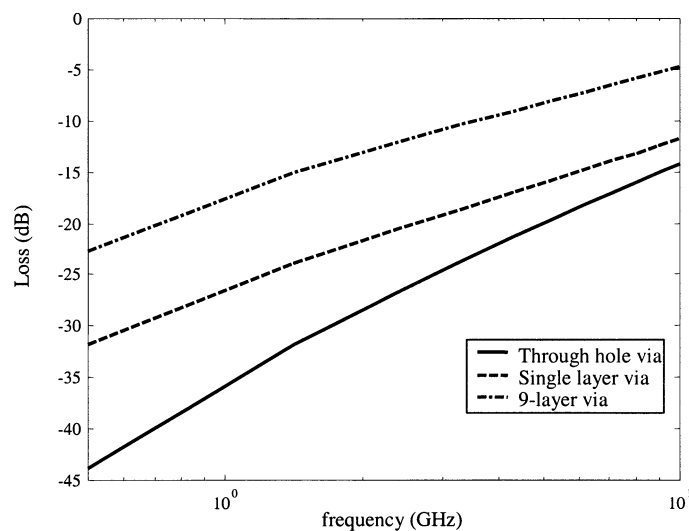


Fig. 6. Loss comparison of three kinds of vias.

into the parallel plate waveguide. The energy is subsequently dissipated or radiated through the edges of the waveguide. It is noted that the power loss for the interior problem computed by the proposed model is only valid for the infinite parallel plates which is assumed in the previous section. They are due to the fact that energy is coupled from the via to the parallel plate waveguide modes. This coupling represents loss from the signal vias. In real-life situations, the finite parallel plates are used and could be connected at their edges for some other applications. The parallel waveguide mode can propagate to the edges of the ground plane and be reflected or be radiated from the edges of the ground plane. This in turn will affect the radiation loss of the signal via. On the other hand, before the waveguide modes reach the edges of the ground plane, they can also be attenuated by dielectric loss in the material and the skin effect loss of the conductors. This will reduce the influence of the edges of the finite ground plane to the signal via radiation.

Fig. 7 shows the loss comparison of a nine-layer vertical via with different layer thicknesses. The parameters are the same

as in Fig. 5, except that the layer thickness of each layer is $d = 0.254, 0.3048, \text{ and } 0.381$ mm. The comparison shows that radiation loss of a nine-layer vertical via increases as the layer thickness increases.

A. Shorting Vias

In the following, we illustrate results for thousands of vias. The via structures are shown in Fig. 1. Two of the vias are connected to differential signaling. There are shorting vias in the neighborhood to reduce coupling. There are many other idle vias on a PCB. The two ends of a shorting via are directly connected to the ground planes. Thus, the voltages of the upper and lower ports of the shorting vias are zero. Let there be two active vias, N_T terminated idle vias, and N_S shorting vias. The total number of vias is

$$N = 2 + N_T + N_S. \quad (75)$$

Let the shorting vias be labeled as $(N_T + 3), (N_T + 4), \dots, (2 + N_T + N_S)$. Then we can rewrite (73) as

$$\begin{aligned} \left(\bar{\bar{F}}_0^{(1)} + \bar{\bar{F}}_0^{(2)} \right) \bar{I}^u &= \left(B_0 \bar{\bar{E}}_0 + \bar{\bar{F}}_0 \bar{\bar{Y}}_{\text{extra}}^{uu} \right)^{(1)} \cdot \bar{\nabla}^u \\ &+ \left(D_0 \bar{\bar{E}}_0 + \bar{\bar{F}}_0 \bar{\bar{Y}}_{\text{extra}}^{ub} \right)^{(1)} \cdot \bar{\nabla}^b \\ &+ \left(B_0 \bar{\bar{E}}_0 + \bar{\bar{F}}_0 \bar{\bar{Y}}_{\text{extra}}^{uu} \right)^{(2)} \cdot \bar{\nabla}^u \\ &+ \left(D_0 \bar{\bar{E}}_0 + \bar{\bar{F}}_0 \bar{\bar{Y}}_{\text{extra}}^{ub} \right)^{(2)} \cdot \bar{\nabla}^b. \end{aligned} \quad (76)$$

In the above matrix equation, the matrices are labeled with superscripts (1) and (2). For matrices with superscript (1), the first $(N_T + 2)$ column elements are their original elements and the others are zeros. For matrices with superscript (2), the last N_S column elements of the matrix are their original elements and the others are zeros. The last N_S elements in the column vectors $\bar{\nabla}^b$ and $\bar{\nabla}^u$ are zeros. Thus, the last two terms on the right-hand side of the equation will be zero.

Note that there is no exterior part for the shorting vias and thus no corresponding exterior problem. Substituting \bar{V}^u , \bar{V}^b , and \bar{T}^u into the above equations and rearranging, we have

$$\begin{aligned} & \left[\bar{F}_0^{(1)} \left(-\bar{Y}_{\text{ant}} + \bar{Y}_{\text{extra}}^{uu} + \bar{Y}_{\text{extra}}^{ub} \right) + (B_0 + D_0) \bar{E}_0^{(1)} \right] \bar{T}_{\text{ant}}^{-1} \\ & \cdot \bar{B}^u + \bar{F}_0^{(2)} \bar{T}^u \\ & = \left[-\bar{F}_0^{(1)} \left(\bar{T}_{\text{sc}} + \bar{Y}_{\text{ant}} \bar{T}_{\text{ant}}^{-1} \bar{T}_{\text{sc}} \right) \right. \\ & \quad - \left(B_0 \bar{E}_0^{(1)} + \bar{F}_0^{(1)} \bar{Y}_{\text{extra}}^{uu} \right) \bar{T}_{\text{sc}} \\ & \quad - \left(D_0 \bar{E}_0^{(1)} + \bar{F}_0^{(1)} \bar{Y}_{\text{extra}}^{ub} \right) \bar{T}_{\text{ant}}^{-1} \bar{T}_{\text{ratio}} \left. \right] \cdot \bar{A}^u \\ & + \left(D_0 \bar{E}_0^{(1)} + \bar{F}_0^{(1)} \bar{Y}_{\text{extra}}^{ub} \right) \bar{T}_{\text{ant}}^{-1} \left[\bar{T}_{\text{sc}} - \bar{T}_{\text{ratio}} \right] \cdot \bar{A}^b. \end{aligned} \quad (77)$$

Note that there are N unknowns in total in the above equation. The first $(N_T + 2)$ unknowns are elements of \bar{B}^u and the rest of the N_S unknowns are elements of \bar{T}^u .

B. Differential and Common Modes

Consider two active vias 1 and 2, so that $N = 2$. This is a four-port problem with four ports labeled as 1_u , 1_b , 2_u , and 2_b . Vias are labeled as 1 and 2 and ports are further labeled as upper and bottom ports

$$\begin{bmatrix} B^{1u} \\ B^{2u} \\ B^{1b} \\ B^{2b} \end{bmatrix} = \begin{bmatrix} S_{1u1u} & S_{1u2u} & S_{1u1b} & S_{1u2b} \\ S_{2u1u} & S_{2u2u} & S_{2u1b} & S_{2u2b} \\ S_{1b1u} & S_{1b2u} & S_{1b1b} & S_{1b2b} \\ S_{2b1u} & S_{2b2u} & S_{2b1b} & S_{2b2b} \end{bmatrix} \begin{bmatrix} A^{1u} \\ A^{2u} \\ A^{1b} \\ A^{2b} \end{bmatrix}.$$

For the differential mode, $A^{1u} = 1/2$, $A^{2u} = -1/2$, and $A^{1b} = A^{2b} = 0$. The reflection coefficient is $R = B^{1u} - B^{2u} = (S_{1u1u} - S_{1u2u} - S_{2u1u} + S_{2u2u})/2$. The transmission coefficient is $T = B^{1b} - B^{2b} = (S_{1b1u} - S_{1b2u} - S_{2b1u} + S_{2b2u})/2$. For the common mode, $A^{1u} = 1$, $A^{2u} = 1$, and $A^{1b} = A^{2b} = 0$. The reflection coefficient is $R = B^{1u} = S_{1u1u} + S_{1u2u}$. The transmission coefficient is $T = B^{1b} = S_{1b1u} + S_{1b2u}$.

In the numerical results, we consider two active vias in either the common mode or the differential mode. In Fig. 8, the transmission and reflection of two coupled active vias for common and differential modes are shown. The magnitudes of reflection and transmission coefficients are plotted as a function of frequency. For this case, we consider the effects of both interior and exterior coupling. Parameters are: via inner radius $a = 0.127$ mm, via outer radius $b = 0.381$ mm, separation of the two vias $s = 1.016$ mm, and layer thickness $h = 2.286$ mm. The material permittivity is $\epsilon = 2.2\epsilon_0$. It can be seen that transmission for the differential mode is larger than the common mode, particularly at high frequency. At very low frequency, the results for the exterior problem lose accuracy because of the thin wire approximation. For more accurate results, we recently have used a realistic trace to model the transmission line that is bent into the exterior part of the via [20]. The trace results show that the reflection will decrease as frequency decreases [20]. The more complicated cases of traces and bent wires in layered media are presently being studied.

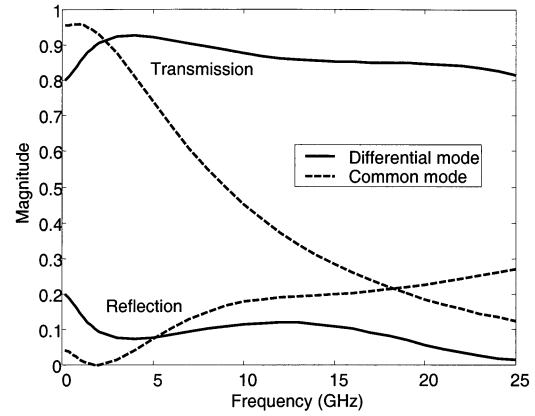


Fig. 8. The transmission and reflection characteristics of two vias in differential signaling.

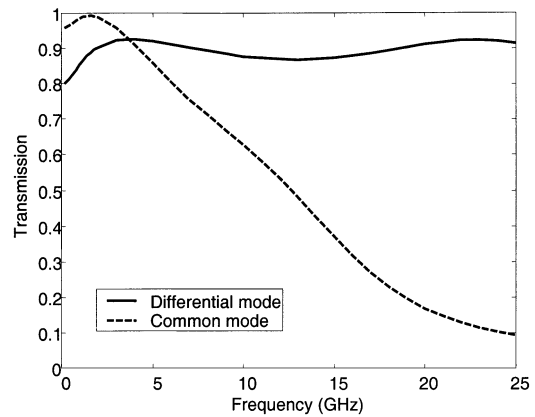


Fig. 9. The transmission characteristics of four vias with two shorted, in differential and common modes.

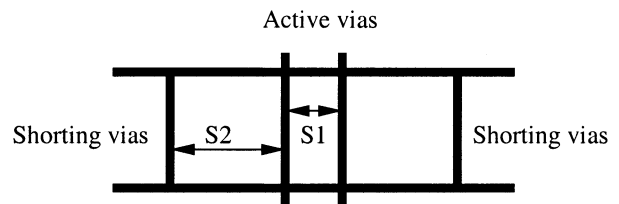


Fig. 10. The geometry of four vias. Two of them are active and two are shorted.

Shorting vias are put in the neighborhood of the active vias to reduce the power loss. In Fig. 9, the transmission of two coupled vias with two shorting vias is plotted as a function of frequency. The geometry is shown in Fig. 10. The four vias are put in a row, with two active vias in the middle and the two shorting vias at the two ends. The separation of the two active vias is $s_1 = 1.016$ mm and the separation of the active and the shorting vias is $s_2 = 2.032$ mm. Other parameters of vias are the same as in Fig. 8. It can be seen that transmission increases for both modes when compared with the case without shorting vias (Fig. 8). To compare the losses with and without shorting vias, the power loss for this four-via case is plotted in Fig. 11. Here, power loss is defined as $1 - P_{\text{trans}} - P_{\text{refl}}$. The dashed and solid lines are for the case of two active vias without shorting vias. The dashed-circle and solid-circle lines are for the case of four vias with two shorted. Fig. 11 shows that the shorting vias can reduce the

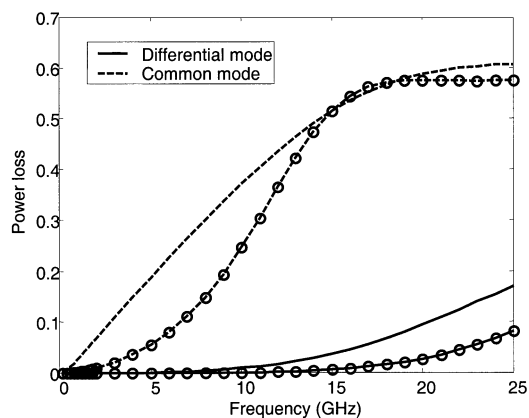


Fig. 11. Comparison of loss with and without shoring vias; circled lines are with shoring vias.

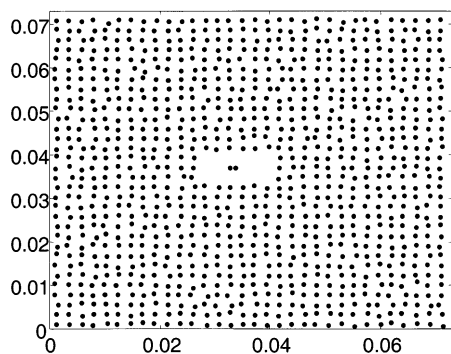


Fig. 12. Locations of the 1008 vias with two signal vias at the center. The labeling of the axes is in meters.

power loss for both differential and common modes, particularly at low frequency.

Next we treat the cases of thousands of vias. The structure for the numerical simulations are shown in Fig. 1. Two of the vias are connected to the signal wires for differential signaling of the common or differential mode. There are shoring vias in the neighborhood to reduce coupling. Furthermore, there can be many other vias labeled as idle terminated vias on the PCB that might influence the signal integrity.

Now we show the capability of the proposed approach to calculate the interactions among a large number of vias. Fig. 12 shows the distribution of 1008 vias and two signal vias at the center. A similar distribution is generated for 2447 vias. The surrounding idle or shoring vias are randomly distributed with a fractional volume of 1%, where the fractional volume $f = n_0 \pi a^2$ and n_0 is the number of vias per unit area. The inner radius of the vias is 0.127 mm, the outer radius of the vias is 0.381 mm, and the separation between two signal vias is 1.016 mm. Fig. 13 shows the power loss of two active vias surrounded with randomly distributed 1006 and 2445 idle vias, for the differential and common modes. It can be seen that the increase of number of idle vias has a small effect on the loss of active vias. The loss in the common mode is larger than that in the differential mode. The same cases are plotted in Figs. 14 and 15 with all the idle vias replaced by shoring vias. Comparing

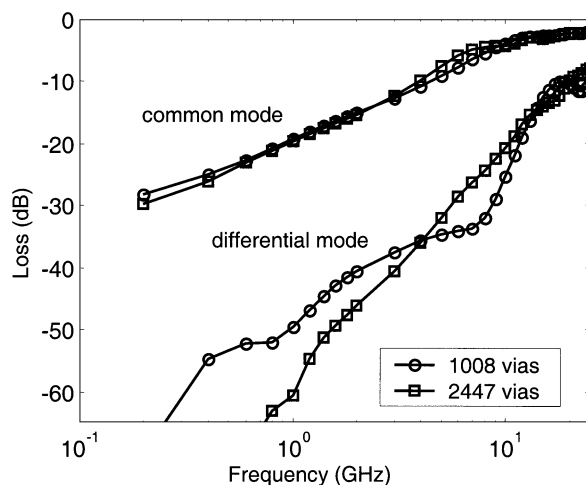


Fig. 13. Comparison of loss between different numbers of vias (differential and common modes).

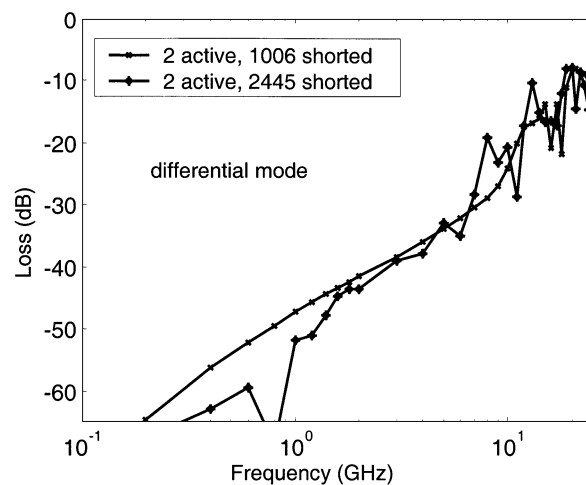


Fig. 14. Comparison of loss between different numbers of shoring vias (differential mode).

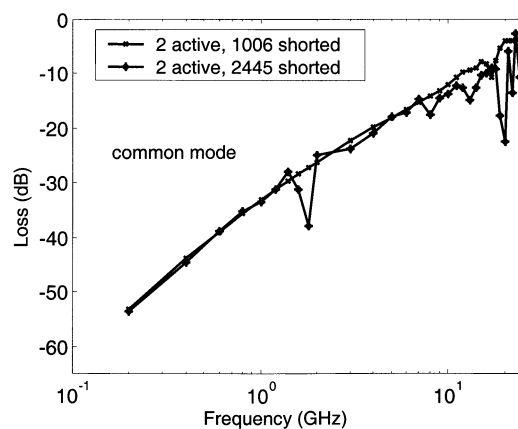


Fig. 15. Comparison of loss between different numbers of shoring vias (common mode).

with Fig. 13, the power loss is greatly reduced for both common and differential modes because the shoring vias provide additional paths for the return currents.

VI. CONCLUSION

The method presented in this paper can be applied to the via discontinuity problem with thousands of vias in high-speed circuit from very low to very high frequency with modest CPU and memory. It starts from the formulation of Green's function of a cylindrical scatterer between parallel plate waveguides and relates the exciting, incident, and scattered waves from each cylinder by Foldy-Lax equations. The interior problem gives the admittance matrix and is related to the exterior problem by equating the port voltages and currents. In this paper, the system matrix of the interior and exterior problem is further combined to give a total matrix of system to be solved by iterative method.

Numerical results are obtained for vias in different configurations and for differential signaling. The simulation technique is also used to solve the coupling problem in multivia structure.

REFERENCES

- [1] A. Djordjevic and T. K. Sarkar, "Computation of inductance of simple vias between two striplines above a ground plane," *IEEE Trans. Microwave Theory Tech.*, vol. MTT-33, pp. 268–269, Mar. 1985.
- [2] A. E. Ruehli, "Equivalent circuit models for three-dimensional multiconductor systems," *IEEE Trans. Microwave Theory Tech.*, vol. MTT-22, pp. 216–221, Mar. 1974.
- [3] T. Wang, R. F. Harrington, and J. R. Mautz, "Quasistatic analysis of a microstrip via through a hole in a ground plane," *IEEE Trans. Microwave Theory Tech.*, vol. 36, pp. 1008–1013, June 1988.
- [4] P. Kok and D. D. Zutter, "Capacitance of a circular symmetric model of a via hole including finite ground plane thickness," *IEEE Trans. Microwave Theory Tech.*, vol. 39, pp. 1229–1234, July 1991.
- [5] P. A. Kok and D. D. Zutter, "Scalar magnetostatic potential approach to the prediction of the excess inductance of grounded vias and vias through a hole in a ground plane," *IEEE Trans. Microwave Theory Tech.*, vol. 42, pp. 1229–1237, July 1994.
- [6] J. P. Quine, H. F. Webster, H. H. Glascock, and R. O. Carlson, "Characterization of via connections in silicon circuit boards," *IEEE Trans. Microwave Theory Tech.*, vol. 36, pp. 21–27, Jan. 1988.
- [7] A. W. Mathis, A. F. Peterson, and C. M. Butler, "Rigorous and simplified models for the capacitance of a circularly symmetric via," *IEEE Trans. Microwave Theory Tech.*, vol. 45, pp. 1875–1878, Oct. 1997.
- [8] S. G. Hsu and R. B. Wu, "Full wave characterization of a through hole via using the matrix-penciled moment method," *IEEE Trans. Microwave Theory Tech.*, vol. 42, pp. 1540–1547, Aug. 1994.
- [9] —, "Full-wave characterization of a through hole via in multi-layered packaging," *IEEE Trans. Microwave Theory Tech.*, vol. 43, pp. 1073–1081, May 1995.
- [10] Q. Gu, Y. E. Yang, and M. A. Tassoudji, "Modeling and analysis of vias in multilayered integrated circuits," *IEEE Trans. Microwave Theory Tech.*, vol. 41, pp. 206–214, Feb. 1993.
- [11] Q. Gu, A. Tassoudji, S. Y. Poh, R. T. Shin, and J. A. Kong, "Coupled noise analysis for adjacent vias in multilayered digital circuits," *IEEE Trans. Circuits Syst.*, vol. 41, pp. 796–804, Dec. 1994.
- [12] D. V. Otto, "The admittance of cylindrical antennas driven from a coaxial line," *Radio Sci.*, vol. 2, no. 9, pp. 1031–1042, 1967.
- [13] E. Laermans, J. D. Geest, D. D. Zutter, F. Olyslager, S. Sercu, and D. Morlion, "Modeling differential via holes," *IEEE Trans. Adv. Packag.*, vol. 24, pp. 357–363, Aug. 2001.
- [14] L. Tsang, H. Chen, C. Huang, and V. Jandhyala, "Modeling of multiple scattering among vias in planar waveguide using Foldy-Lax equations," *Microwave Opt. Technol. Lett.*, vol. 31, no. 3, pp. 201–208, Nov. 2001.
- [15] L. Tsang, K. H. Ding, G. Zhang, C. Hsu, and J. A. Kong, "Backscattering enhancement and clustering effects of randomly distributed dielectric cylinders overlying a dielectric half space based on Monte Carlo simulations," *IEEE Trans. Antennas Propagat.*, vol. 43, pp. 488–499, May 1995.
- [16] L. Tsang, J. A. Kong, and K. H. Ding, *Scattering of Electromagnetic Waves: Vol. 1 Theory and Applications*. New York: Wiley Interscience, 2000.
- [17] L. Tsang, J. A. Kong, K. H. Ding, and C. Ao, *Scattering of Electromagnetic Waves: Vol. 2 Numerical Simulations*. New York: Wiley Interscience, 2001.
- [18] Y. B. Hua and T. K. Sarkar, "Generalized pencil-of-function method for extracting poles of an EM system from its transient response," *IEEE Trans. Antenna Propagat.*, vol. 37, pp. 229–234, Feb. 1989.
- [19] R. F. Harrington, *Field Computation by Moment Methods*. New York: Macmillan.
- [20] H. F. Chen, "Fast electromagnetic simulation for interconnects on high speed circuits," Ph.D. dissertation, Dept. Elect. Eng., Univ. Washington, Seattle, WA, 2002.

Houfei Chen was born on October 27, 1973, in Shanghai, China. He received the B.S. and M.S. degrees from the University of Science and Technology of China, Hefei, China, in 1995 and 1998, respectively, and the Ph.D. degree from the University of Washington, Seattle, in 2002, all in electrical engineering.

He is currently a Development Engineer with the Advance System Research Laboratory, MICRON, Boise, ID.

Qin Li received the B.S. and M.S. degrees in space physics from Wuhan University, Wuhan, China, in 1985 and 1988, respectively, and the Ph.D. degree in electrical engineering from the University of Washington, Seattle, in 2000.

He was a Post-Graduate Researcher with the Institute for Computational Earth System Sciences, University of California at Santa Barbara, for one year. He is currently a Research Assistant Professor with the Department of Electrical Engineering, University of Washington.

Leung Tsang (S'73–M'75–SM'85–F'90) was born in Hong Kong. He received the S.B., S.M., and Ph.D. degrees from the Massachusetts Institute of Technology (MIT), Cambridge.

He is a Professor of Electrical Engineering with the Department of Electrical Engineering, University of Washington, Seattle, where he has taught since 1983. Beginning in September 2001, he has been on leave from the University of Washington and is a Professor Chair and Assistant Head with the Department of Electronic Engineering, City University of Hong Kong. He coauthored: *Theory of Microwave Remote Sensing* (New York: Wiley-Interscience, 1985), *Scattering of Electromagnetic Waves, Vol. 1: Theory and Applications*, (New York: Wiley Interscience, 2000), *Scattering of Electromagnetic Waves Vol. 2: Numerical Simulations* (New York: Wiley Interscience, 2001) and *Scattering of Electromagnetic Waves Vol. 3: Advanced Topics* (New York: Wiley Interscience, 2001). His current research interests include wave propagation in random media and rough surfaces, remote sensing, high-speed interconnects, computational electromagnetics, wireless communications, and optoelectronics.

Dr. Tsang is a Fellow of the Optical Society of America. From 1996 to 2001, he was the editor-in-chief of the IEEE TRANSACTIONS ON GEOSCIENCE AND REMOTE SENSING. He was the Technical Program chairman of the 1994 IEEE Antennas and Propagation International Symposium and URSI Radio Science Meeting and the 1995 Progress in Electromagnetics Research Symposium. He was the general chairman of the 1998 IEEE International Geoscience and Remote Sensing Symposium. He is an Administrative Committee (AdCom) member of the IEEE Geoscience and Remote Sensing Society. He was the recipient of the IEEE Geoscience and Remote Sensing Society Outstanding Service Award in 2000 and the IEEE Third Millennium Medal in 2000.

Chung-Chi Huang received the B.S. degree in mechanical engineering and M.S. degree in computer science and engineering from the National Sun Yat-sen University, Kaohsiung, Taiwan, R.O.C., in 1994 and 1996, respectively, and is currently working toward the Ph.D. degree at the University of Washington, Seattle.

His current interests include layered medium Green's function, high-speed interconnects, and computational electromagnetics.

Vikram Jandhyala (S'91–M'95) received the B.Tech. degree in electrical engineering from the Indian Institute of Technology, Delhi, India, in 1993, and the M.S. and Ph.D. degrees from the University of Illinois at Urbana-Champaign (UIUC), in 1995 and 1998, respectively. As part of his graduate work, he codeveloped the steepest descent fast-multipole method.

He is currently an Assistant Professor with the Department of Electrical Engineering, University of Washington, Seattle. His research interests include several aspects of computational and applied electromagnetics, including integral equation techniques, fast computational algorithms, high-speed circuits and devices, coupled simulation, signal integrity, and scattering computation. From 1998 to 2000, he was a Research and Development Engineer with the Ansoft Corporation, Pittsburgh, PA. He was involved in the acceleration of Ansoft's integral equation solvers and codeveloped a fast-multipole-based integral-equation solver for Ansoft's Spicelink version 4.0, which was released in June 1999. He has authored a book chapter and over 60 journal papers and papers in refereed conference proceedings.

Dr. Jandhyala is a full member of URSI Commission B. He has served as a reviewer for several IEEE transactions and conferences. He was the recipient of the National Science Foundation CAREER Grant (2001), an Outstanding Graduate Research Award presented by UIUC (1998), and an IEEE Microwave Graduate Fellowship (1996–1997).